LBL-12667
Preprint

Submitted to Nuclear Physics

A RELATIVISTIC QUANTUM FIELD THEORETICAL MODEL FOR NUCLEAR SLAB COLLISION DYNAMICS

K.-H. Müller

May 1981

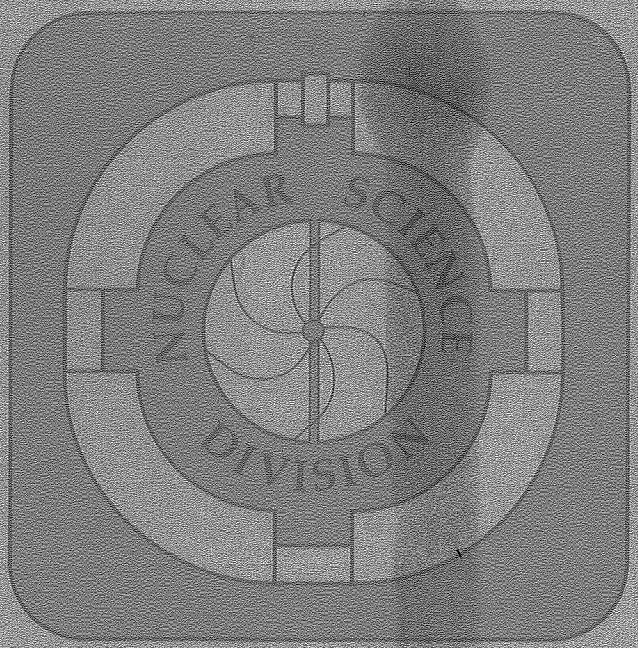

Prepared for the U.S. Department of Energy under Contract W-7405-ENG-48

DISCLAIMER

LBL-12667

A Relativistic Quantum Field Theoretical Model for Nuclear Slab Collision Dynamics*

K.-H. Müller

Nuclear Science Division
Lawrence Berkeley Laboratory
University of California
Berkeley, CA 94720

Abstract

We treat the dynamics of colliding nuclear slabs in a relativistic quantum field theory by using the relativistic mean field approximation. Starting from Walecka's Lagrangian, the nucleons are represented by single particle spinors determined by a Dirac equation that contains a repulsive mean vector meson field and an attractive mean scalar meson field. Both fields satisfy Klein-Gordon equations whose source terms are again determined by the nucleon spinors. The two equal nuclear slabs are translationally invariant in two transverse dimensions and consist of spin and isospin symmetric nuclear matter. By specification of appropriate initial conditions for the collision, we numerically solve the system of coupled Dirac and Klein-Gordon equations for lab energies per nucleon up to 420 MeV. For small energies the results are similar to TDHF results. The time dependence of the density distribution, the mean meson fields, and the damping of the collision are studied. At the highest bombarding energy retardation effects are taken into account.

*This work was supported by the Deutsche Forschungsgemeinschaft, 5300 Bonn-Bad Godesberg, West Germany and by the Director, Office of Energy Research, Division of Nuclear Physics of the Office of High Energy and Nuclear Physics of the U.S. Department of Energy under Contract W-7405-ENG-48.

A Relativistic Quantum Field Theoretical Model for Nuclear Slab Collision Dynamics

Table of Contents

I. Introduction

One of the goals of heavy ion physics is to study the properties of nuclear matter under extreme conditions, which means at high excitation and high density, trying to discover novel phenomena. It is therefore of great interest to study the evolution of a nucleus-nucleus collision process in a model that has no latitude for an arbitrary selection of collective coordinates or any ad hoc parametrization of the dynamics. At low bombarding energies. i.e., $E_{c.m.}/A < 10$ MeV, the TDHF-model is a very reasonable microscopic model that leads to a good understanding of the dynamical aspects of the fusion and deep inelastic reaction mechanism[1]. Since one solves in the TDHF-model a time-dependent Schrödinger equation using a static nucleon-nucleon interaction, this model is naturally restricted to nonrelativistic heavy ion collisions. At relativistically high bombarding energies, the cascade model[2] and the nuclear fluid-dynamical model[3] can describe many observed quantities of a relativistic heavy ion collision. But still the nuclear collision dynamics at intermediate and high energies are not very well understood. At these energies a quantum field theoretical model for the colliding many-body system on the basis of interacting time-dependent fermion and meson fields can give interesting insight in the collision dynamics.

We introduce in this paper Walecka's relativistic quantum field theoretical mean field model[4] in its time-dependent version to describe the collision of two nuclear slabs. We shall show that this model is in a sense an extension of the TDHF-model to relativistic energies. The justification to describe large amplitude nuclear dynamics in this time dependent relativistic mean field model (TDRMF-model) is established by the recent successes of the static relativistic mean field model in describing

the properties of static nuclear matter[4,5] and the structure of static finite nuclei[6-8]. The organization of this paper is as follows.

In Sec. II the general formalism of the relativistic quantum field theoretical model is reviewed and the mean field approximation is introduced. In order to limit the computational scope, we have restricted our formalism to the dynamics of two equal colliding slabs of spin and isospin symmetric nuclear matter. We show in Sec. III that the problem reduces to a set of coupled nonlinear equations of Dirac and Klein-Gordon type for time-dependent spinors of a single spatial variable. In Sec. IV we introduce the Yukawa coupling constants and masses of the mesons and present the results of the static slab calculation. How to specify the initial condition is discussed in Sec. V. In Sec. VI we critically ask for the possible validity of the model, and the results for the collision processes are discussed. Finally, in Sec. VII we give a brief summary and discuss possibilities for future work that appears promising. The numerical methods we used are described in the appendix.

II. The Relativistic Field Theory of Nuclear Matter

A. The General Formalism

As long as the intrinsic quark structure in a nuclear matter system can be ignored--that means as long as the nucleon bags do not overlap--one should be able to present the interaction between nucleons by introducing a set of meson fields of various spin and isospin with Yukawa coupling to the nucleons. A model based on the first two chargeless mesons, the sigma-(σ) and the omega-meson (V_μ), was introduced first by Johnson and Teller[9] and by Duerr[10]. Later Walecka and collaborators[4,11] intensively investigated the model.

For describing the collision of two slabs of spin and isospin symmetric nuclear matter, we introduce as in the standard Walecka model the neutral scalar σ-field and the neutral vector meson V_μ-field. The Coulomb field is neglected. The Lagrangian density of the Walecka model is

$$\mathcal{L} = -\bar{\psi}(\gamma_\mu \partial_\mu + m)\psi - \frac{1}{2}(\partial_\mu \underset{\sim}{\sigma})^2 - \frac{1}{2}m_s^2 \underset{\sim}{\sigma}^2 - \frac{1}{4}F_{\mu\nu}F_{\mu\nu}$$
$$- \frac{1}{2}m_V^2 \underset{\sim\mu}{V}\underset{\sim\mu}{V} - g_s\bar{\psi}\psi\underset{\sim}{\sigma} + ig_V\bar{\psi}\gamma_\mu\psi\underset{\sim\mu}{V} \qquad (1)$$

where

$$F_{\mu\nu} = \partial_\mu \underset{\sim\nu}{V} - \partial_\nu \underset{\sim\mu}{V}$$

γ_μ are the usual γ-matrices, g_s and g_V Yukawa coupling constants, m_s and m_V the scalar and vector meson masses, m is the nucleon mass. ψ is the fermion field. While the first five terms in the Lagrangian are the free Lagrangians for the fermion and meson fields, the last two terms determine the interaction between the fermion field and the meson fields.

With the above Lagrangian density the Euler-Lagrange equations yield the following coupled field equations.

$$\{-\gamma_\mu \partial_\mu - m - g_s \underset{\sim}{\sigma} + i g_v \gamma_\mu \underset{\sim}{V}_\mu\}\psi = 0 \tag{2a}$$

$$(-\Box + m_s^2)\underset{\sim}{\sigma} = -g_s \bar{\psi}\psi \tag{2b}$$

$$(-\Box + m_v^2)\underset{\sim}{V}_\mu + \partial_\mu \partial_\nu \underset{\sim}{V}_\nu = i g_v \bar{\psi}\gamma_\mu \psi \ . \tag{2c}$$

Taking into account that the nucleon current is conserved, the Proca Eq. (2c) is equivalent to the Klein-Gordon equation

$$(-\Box + m_v^2)\underset{\sim}{V}_\mu = i g_v \bar{\psi}\gamma_\mu \psi \tag{2c'}$$

These equations are fully relativistic and Lorentz covariant. In the static approximation the $\underset{\sim}{\sigma}$-field corresponds to an attractive nucleon-nucleon interaction due to a two pion-exchange while the $\underset{\sim}{V}_\mu$-field on the other hand yields a repulsive potential. The strength and range of these interactions are determined by the coupling constants and the meson masses. These two mesons are sufficient to account for the saturation of nuclear matter and a great number of single particle properties of the finite nucleus[9,10].

B. The Mean Field Approximation

As the source currents in (2b) and (2c') are implicit function of $\underset{\sim}{\sigma}$ and $\underset{\sim}{V}_\mu$ because of the Dirac equation (2a) the sets of coupled field operator equations are very intractable in their present form. J.D. Walecka[4] proposed to linearize the Dirac Eq. (2a) by substituting the field operators $\underset{\sim}{\sigma}$ and $\underset{\sim}{V}_\mu$ by their expectation values and to introduce the normal ordering of the operators in the source terms in Eqs. (2b) and (2c). In this mean field approximation, the effects caused by quantum fluctuations about these mean values are neglected. Recent successes in describing the properties of finite nuclei[7] demonstrated that the effects of quantum fluctuations are not very important.

III. The TDRMF-Model for Colliding Nuclear Slabs

A. The Time-Dependent Field Equations

We assume the time-dependent relativistic many-body state $|\phi>$ that describes the system of two equal colliding slabs of spin and isospin symmetric nuclear matter to be of the form $|\phi> = a^+_{\alpha_1} a^+_{\alpha_2} \ldots a^+_{\alpha_A} |0>$. Here A is the number of nucleons in the system. The a^+_α's are nucleon creation operators and $|0>$ is the vacuum. We expand the fermion field ψ in a complete set of time and space dependent Dirac spinor functions f_α and g_α. The time-dependent solutions of the nucleon field can be written as

$$\psi(\vec{x},t) = \sum_\alpha f_\alpha(\vec{x},t) a_\alpha + \sum_\alpha g_\alpha(\vec{x},t) b^+_\alpha \tag{3}$$

where b^+_α is an antinucleon creation operator. With the abbreviations

$$\sigma = <\phi|\underset{\sim}{\sigma}|\phi> \quad , \; V_\mu = <\phi|\underset{\sim}{V}_\mu|\phi> \quad , \; m^* = m + g_s\sigma \tag{4}$$

the mean field approximation leads to the Dirac equation

$$\{-\gamma_\mu \partial_\mu - m^* + ig_V\gamma_\mu V_\mu\} f_\alpha = 0 \tag{5a}$$

where the mean meson fields obey the Klein-Gordon equations

$$(-\Box + m_s^2)\sigma = -g_s<\phi|:\bar{\psi}\psi:|\phi> \equiv -g_s\rho_s \tag{5b}$$

$$(-\Box + m_V^2)V_\mu = ig_V<\phi|:\bar{\psi}\gamma_\mu\psi:|\phi> \equiv g_V j_\mu \tag{5c}$$

Here :: defines normal-ordering[4] of all expressions with respect to the set of operators $a_\alpha, a^+_\alpha, b_\alpha, b^+_\alpha$.

In order to limit the computational scope in this work, we consider here for the nuclear collision the special geometry of two colliding slabs. With moving slabs in z-direction, the system is translational invariant in

the transverse x-y direction and rotational invariant with respect to any axis parallel to the z-axis. Therefore, all expectation values in Eqs. (5) are only functions of the spatial variable z and the time, and it is

$$V_x = V_y = 0 \quad . \tag{6}$$

Using the standard $\vec{\alpha}$ and β matrices, Eq. (5a) gets

$$\left(-i\frac{\partial}{c\partial t} + g_v V_o + \vec{\alpha}\frac{1}{i}\vec{\nabla} - \alpha_z g_v V_z + \beta m^*\right) f_\alpha = 0 \tag{7}$$

V_o is the time component of V_μ. Because of the translational invariance in the transverse direction f_α is a product of a plane wave in transverse coordinates $\vec{x}_\perp$ and a wave function in the z coordinate.

$$f_\alpha = \frac{1}{\sqrt{F}} e^{i\vec{K}_\perp \vec{x}_\perp} f_{jK_\perp}(z,t) \tag{8}$$

F is an infinite normalizing area in the x-y plane. The subscripts j and $K_\perp$ label the z-quantum number and the transverse wave vector $\vec{k}_\perp$.

The relativistic wave function $f_{jK_\perp}$ is a solution of the Dirac equation

$$\left[-i\frac{\partial}{c\partial t} + g_v V_o + \vec{\alpha}_\perp \vec{K}_\perp + \alpha_z\left(\frac{1}{i}\frac{\partial}{\partial z} - g_v V_z\right) + \beta m^*\right] f_{jK_\perp}(z,t) = 0 \quad . \tag{9}$$

As in ref. 12) we diagonalize the hermitian operator $\vec{\alpha}_\perp \vec{K}_\perp + \beta m^*$ by a unitary transformation U. One finds

$$U^+(\vec{\alpha}_\perp \vec{K}_\perp + \beta m^*)U = \beta\sqrt{K_\perp^2 + m^{*2}} \quad . \tag{10}$$

Introducing the functions $\tilde{f}_{A_{jK_\perp}}$ and $\tilde{f}_{B_{jK_\perp}}$ in the form

$$\begin{pmatrix} \chi^\lambda \tilde{f}_{A_{jK_\perp}} \\ \frac{K_x\sigma_z - iK_y}{K_\perp}\chi^\lambda \tilde{f}_{B_{jK_\perp}} \end{pmatrix} = U^+ f_{jK_\perp} \tag{11}$$

where $\chi^1 = \begin{pmatrix}1\\0\end{pmatrix}$ and $\chi^2 = \begin{pmatrix}0\\1\end{pmatrix}$, one gets a system of coupled equations for the large and small components $\tilde{f}_{A_{jK_\perp}}$ and $\tilde{f}_{B_{jK_\perp}}$.

$$\frac{\partial}{c\partial t}\tilde{f}_{A_{jK_\perp}} + \left(\frac{\partial}{\partial z} - ig_v V_z\right)\tilde{f}_{B_{jK_\perp}} = i(-g_v V_o - \sqrt{K_\perp^2 + m^{*2}})\,\tilde{f}_{A_{jK_\perp}} \tag{12a}$$

$$\frac{\partial}{c\partial t}\tilde{f}_{B_{jK_\perp}} + \left(\frac{\partial}{\partial z} - ig_v V_z\right)\tilde{f}_{A_{jK_\perp}} = i(-g_v V_o + \sqrt{K_\perp^2 + m^{*2}})\,\tilde{f}_{B_{jK_\perp}}. \tag{12b}$$

The source terms in (5b) and (5c) can be expressed in terms of the functions $\tilde{f}_{A_{jK_\perp}}$ and $\tilde{f}_{B_{jK_\perp}}$. The scalar density ρ_s, the vector density $\rho_v = j_4$ and the current in z-direction j_z are

$$\rho_s = 4 \sum_j \frac{1}{2\pi} \int dK_\perp K_\perp \frac{m^*}{\sqrt{K_\perp^2+m^{*2}}} \left\{ \left|\tilde{f}_{A_{jK_\perp}}\right|^2 - \left|\tilde{f}_{B_{jK_\perp}}\right|^2 \right\} \tag{13a}$$

$$\rho_v = 4 \sum_j \frac{1}{2\pi} \int dK_\perp K_\perp \left\{ \left|\tilde{f}_{A_{jK_\perp}}\right|^2 + \left|\tilde{f}_{B_{jK_\perp}}\right|^2 \right\} \tag{13b}$$

$$j_z = 4 \sum_j \frac{1}{2\pi} \int dK_\perp K_\perp \left\{ \tilde{f}^*_{A_{jK_\perp}} \tilde{f}_{B_{jK_\perp}} + \tilde{f}_{A_{jK_\perp}} \tilde{f}^*_{B_{jK_\perp}} \right\} \tag{13c}$$

The factor 4 in front of these expressions is due to the spin and isospin degeneracy.

The factorization of the function f_α of Eq. (8) has the consequence that during the slab collision the initial occupation of the transverse wave vector quantum number $K_\perp$ does not change and the integrations in (13) cover at each time the initially fixed domains, which depend themselves on j. As in a one-dimensional TDHF-calculation this omission of freedom of changes in the transverse directions means a rather severe limitation to the relativistic many-body wavefunction and has certainly implications regarding the physical applicability of our calculations.

The concept of calculating the nuclear slab collision in the TDRMF-model is now essentially as follows. With the appropriate initial conditions for the relativistic many-body wavefunction for two approaching nuclear slabs, which will be discussed in Sec. V, we calculate the source terms given by the expressions in Eqs. (13). The meson fields σ, V_0 and V_z are then determined by solving the Klein-Gordon equations

$$\frac{\partial^2\sigma}{c^2\partial t^2} - \frac{\partial^2\sigma}{\partial z^2} + m_s^2\sigma = -g_s\rho_s \tag{14a}$$

$$\frac{\partial^2 V_0}{c^2\partial t^2} - \frac{\partial^2 V_0}{\partial z^2} + m_v^2 V_0 = g_v\rho_v \tag{14b}$$

$$\frac{\partial^2 V_z}{c^2\partial t^2} - \frac{\partial^2 V_z}{\partial z^2} + m_v^2 V_z = g_v j_z \tag{14b}$$

where the scalar density in Eq. (14a) is itself a function of σ. Using these fields in the set of coupled Eqs. (12) we determine the small and large components of the functions $\tilde{f}$ at each point in space at an infinitesimally later time. With these new functions $\tilde{f}$ we calculate the source terms again, and so on. The numerical methods we use to solve these equations are discussed in the appendix.

B. The Total Energy and Momentum

During the collision process the momentum four vector of the system is conserved. This four vector can be expressed in terms of the stress tensor $T_{\mu\nu}$ [4,13].

$$(\vec{P}, \frac{i}{c}E) = \frac{1}{ic}\int d^3x\, T_{4\nu} \tag{15}$$

where

$$T_{\mu\nu} = \left\{ -\frac{1}{2}\left[\left(\frac{\partial\sigma}{\partial x}\right)^2 + m_s^2\sigma^2\right] - \frac{1}{4}F_{\lambda\rho}F_{\lambda\rho} - \frac{m_v^2}{2}V_\lambda V_\lambda \right\}\delta_{\mu\nu}$$

$$+ \bar{\psi}\gamma_\mu \frac{\partial\psi}{\partial x_\nu} + \frac{\partial\sigma}{x_\nu}\frac{\partial\sigma}{x_\mu} - \frac{\partial V_\lambda}{\partial x_\lambda}F_{\lambda\mu} \qquad (16)$$

In the case of colliding slabs this gives for the energy per unit area

$$\frac{E}{F} = \int dz \left\{ i\langle\phi|:\psi^+ \frac{\partial}{c\partial t}\psi:|\phi\rangle \right.$$

$$+ \frac{m_s^2}{2}\sigma^2 + \frac{1}{2}\left(\frac{\partial\sigma}{c\partial t}\right)^2 + \left(\frac{\partial\sigma}{\partial z}\right)^2 + \frac{1}{2}\left(\frac{\partial V_z}{c\partial t}\right)^2 - \frac{1}{2}\left(\frac{\partial V_o}{\partial z}\right)^2$$

$$\left. - \frac{1}{2}m_v^2V_o^2 + \frac{1}{2}m_v^2V_z^2 \right\} . \qquad (17)$$

For the momentum per unit area one gets

$$\frac{P_z}{F} = \frac{1}{c}\int dz \left\{ \langle\phi|:\psi^+ \frac{1}{i}\frac{\partial}{\partial z}\psi:|\phi\rangle - \frac{\partial\sigma}{c\partial t}\frac{\partial\sigma}{\partial z} - \frac{\partial V_z}{\partial z}\left(\frac{\partial V_o}{\partial z} + \frac{\partial V_z}{c\partial t}\right)\right\}. \qquad (18)$$

The first part of the integrant belongs to the nucleon momentum density; the last two parts refer to the momentum density caused by the meson fields. An instructive quantity is the half side momentum per unit area, which we define by integration only along the positive z-axis. After the collision, if the slabs are separated again, this quantity determines the intrinsic excitation of the system.

IV. The Static Slab

A. Parameters, Formalism and Results

First of all, we want to specify the parameters in the model, which are the Yukawa coupling constants g_s and g_v as well as the sigma-meson mass m_s and the omega-meson mass m_v. It was shown by J. Boguta[7] that the mass of the sigma-meson is determined in the static mean field calculation for nuclei by fitting the surface thickness of the nucleus. An acceptable range is 500 MeV $\leq m_s \leq$ 525 MeV. As in ref. 7), we choose m_s = 500 MeV and for the omega-meson mass m_v = 780 MeV. The ratios $C_s = (g_s/m_s)m$ and $C_v = (g_v/m_v)m$ are determined by the binding energy per nucleon in infinite symmetric nuclear matter at saturation density. With a saturating Fermi momentum of $K_F = 1.34$ fm^{-1} and a corresponding energy per nucleon of -15.75 MeV, one gets $C_s = 17.95$ and $C_v = 15.60$. These parameters are similar to those determined by J.D. Walecka[4]. We use the above enumerated values of the coupling constants and masses to solve the static slab problem as well as the dynamical collision problem.

To calculate the nuclear collisions of two equal slabs in the c.m. frame, we have to prepare the appropriate initial condition for slabs approaching with a certain velocity. As the Dirac equation is Lorentz covariant, the initial spinors can be constructed from the static spinors by an inhomogeneous Lorentz transformation. Therefore, we first consider the problem of a static nuclear slab. In order to construct a solution we have to solve self-consistently the static Dirac equation.

$$\frac{\partial}{\partial z}\tilde{f}_{B_{jK_\perp}} = i(\varepsilon_{jK_\perp} - g_v V_o - \sqrt{K^2 + m^{*2}})\,\tilde{f}_{A_{jK_\perp}} \tag{19a}$$

$$\frac{\partial}{\partial z}\tilde{f}_{A_{jK_\perp}} = i(\varepsilon_{jK_\perp} - g_v V_o + \sqrt{K^2 + m^{*2}})\,\tilde{f}_{B_{jK_\perp}} \tag{19b}$$

$\varepsilon_{jK_\perp}$ is the single nucleon energy including its rest-mass in a state characterized by the quantum numbers j and $K_\perp$. With the replacement

$$\hat{f}_{B_{jK_\perp}} = i\,\tilde{f}_{B_{jK_\perp}} \tag{20}$$

the system (19) becomes purely real. The relativistic many-body ground state of the slab will correspond to the occupation of all single nucleon states with energy $\varepsilon_{jK_\perp}$ below the energy $\varepsilon_F + m$, where ε_F is the Fermi energy. A constraint to the self-consistent procedure is that the number of nucleons per unit area in the x-y plane, defined as

$$\frac{A}{F} = \int_{-\infty}^{\infty} \rho_V(z)dz \tag{21}$$

remains constant. Since the spinors are normalized to one we get by using Eq. (13b)

$$\frac{A}{F} = \frac{1}{\pi} \sum_{j}^{N} K_{\perp\,max}^2(j) \quad . \tag{22}$$

Here $K_{\perp\,max}$ is the maximum transverse momentum defined by

$$\varepsilon_{jK_{\perp\,max}} = \varepsilon_F + m \quad . \tag{23}$$

The sum in Eq. (22) is therefore restricted to those z-quantum numbers where $\varepsilon_{jo} \leqslant \varepsilon_F + m$. N is the number of possible z-quantum numbers. Numerically we found

$$\varepsilon_{jK_\perp} \cong \varepsilon_{jo} + \frac{K_\perp^{\,2}}{2\langle m^* \rangle} \tag{24}$$

where

$$\langle m^* \rangle = \frac{\int \rho_V m^* dz}{\int \rho_V dz} \tag{25}$$

This is due to the fact that the transverse kinetic energy of the nucleons is small compared to its average effective mass <m*>.

With Eq. (24) one gets instead of (22) the constraint

$$\frac{A}{F} = \frac{1}{\pi} \sum_{j}^{N} 2\langle m^* \rangle (\varepsilon_F + m - \varepsilon_{jo}) \quad . \tag{26}$$

The dependence of the functions $\tilde{f}_{B_{jK_\perp}}$ and $\tilde{f}_{A_{jK_\perp}}$ on the transverse wave number causes a substantial numerical complication and lets the problem appear numerically as a two-dimensional one. To avoid this complication we take advantage of the rather weak dependence of the functions $\tilde{f}_A$ and $\tilde{f}_B$ on $K_\perp$ and consider for simplicity these functions at only one constant value of $K_\perp$, namely, $K_\perp = 0$. This approximation, as we will show, leads to a very appropriate result for the static slab. As the slab collision geometry omits in an unrealistic way the freedom of changes in the transverse direction and $K_\perp$ therefore appears as an unreal, artificial quantum number, the above approximation is directly suggested. Therefore, we use the approach

$$\tilde{f}_{A/B_{jK_\perp}} \simeq \tilde{f}_{A/B_{j0}} \quad . \tag{27}$$

Thus, while the structure of the resulting problem is no more difficult computationally than a genuine one-dimensional problem, we may use the three-dimensional phase space and the Yukawa coupling constants as well as the meson masses determined by earlier three-dimensional static calculations for spherical nuclei.

With Eq. (27) the integrals in Eqs. (13) can easily be performed and the scalar and vector densities become

$$\rho_s = \frac{2}{\pi} \sum_j^N m^* \left\{ \sqrt{K_{\perp\,max}^2 + m^{*2}} - |m^*| \right\} \left\{ |\tilde{f}_{A_{j0}}|^2 - |\tilde{f}_{B_{j0}}|^2 \right\} \tag{28a}$$

$$\rho_v = \frac{1}{\pi} \sum_j^N K_{\perp\,max}^2 \left\{ |\tilde{f}_{A_{j0}}|^2 + |\tilde{f}_{B_{j0}}|^2 \right\} . \tag{28b}$$

In the static case the solutions of the Klein-Gordon Eqs. (14a) and (14b) can be expressed in terms of Greensfunctions[12]. One obtains

$$\sigma(z) = \frac{-g_s}{2m_s} \int e^{-m_s|z-z'|} \rho_s(z')dz' \tag{29a}$$

$$V_0(z) = \frac{g_v}{2m_v} \int e^{-m_v|z-z'|} \rho_v(z')dz' \quad . \tag{29b}$$

As $\rho_s(z')$ depends on $\sigma(z')$ because of Eq. (28a), the above Eq. (29a) is an integral equation for σ.

Now, the concept of finding the self-consistent static slab solution is as follows. For a given number of nucleons per unit area we assume appropriate vector and scalar densities ρ_v and ρ_s. With these we determine the integral in Eq. (29b) and solve the integral equation (29a). With the resulting meson fields the eigenvalue problem (19) with regard to the boundary condition for the wavefunctions is solved. The constraint of Eq. (26) determines the maximum transverse momenta and the number of occupied states. Then by using Eqs. (28) new vector and scalar densities are determined. We go through this procedure until self-consistency is reached.

We discuss now the numerical results we get for the static slab. To compare our results with those one obtains from a corresponding TDHF-slab calculation, we choose for the number of nucleons per unit area A/F = 1.4 fm^{-2}. This is the value for which most of the slab collision

calculations in ref. 14) have been done. As in ref. 14) we find the number N of occupied z-quantum numbers to be 4. The Fermi energy in our case is -10.43 MeV. The average effective mass $\langle m^* \rangle$ has the value 545 MeV. J.D. Walecka[4] got for infinite nuclear matter ($K_F = 1.42$ fm^{-1}) for the effective mass $m^* = 526$ MeV. The single particle energies ε_{j0} as well as the maximum occupied transverse momentum $K_{\perp max}$ are listed in table 1. That the low-lying states are stronger bound than in a nonrelativistic Hartree calculation is a characteristic of the relativistic mean field model[7]. Here this is even reinforced by the approximation (27), which leads to a smaller thickness and a higher central density of the system than one would actually get.

Figure 1 shows the large and small components of the relativistic nucleon wavefunctions. Figure 2 displays the nucleon density ρ_v and the scalar density ρ_s. Because of reflection symmetry with respect to the slab center, only half of each distribution is plotted. The thickness of the slab corresponds to a nucleus with $A \simeq 35$. That the density distributions show almost no fluctuations is because the higher lying orbits are much less weighted than the lower ones. This is clearly seen from Eqs. (28). The small components in the wavefunctions even smooth the densities. Because of the smallness of the small component the scalar density is similar to the vector density. This is different in the case of colliding slabs having velocities close to the velocity of light. Figure 3 shows the strengths of the scalar field and the time component of the vector field. Both fields have opposite signs and are in its absolute value almost an order of magnitude larger than a nonrelativistic single particle potential.

B. Relation to the Nonrelativistic Hartree Concept

We want to rewrite the system of Eqs. (19) to see the relation to a nonrelativistic Hartree calculation. Expressing the small component in Eqs. (19) in terms of the large component, one obtains a Schrödinger equation for $\tilde{f}_{A_{j0}}$ with a single particle potential U_{eff}.

$$-\frac{1}{2m}\frac{\partial^2}{\partial z^2}\tilde{f}_{A_{j0}} + U_{eff}\,\tilde{f}_{A_{j0}} = (\varepsilon_{j0} - m)\tilde{f}_{A_{j0}} \tag{30}$$

Here

$$U_{eff} = g_s\sigma + g_v V_o - \frac{g_v^2 V_o^2 - g_s^2\sigma^2}{2m} + \frac{1}{2mx}\left(\frac{\partial}{\partial z}x\right)\frac{\partial}{\partial z} + \frac{g_v V_o}{m}(\varepsilon_{j0} - m) - \frac{(\varepsilon_{j0}-m)^2}{2m} \tag{31}$$

and

$$x = \varepsilon_{j0} - g_v V_o + |m^*| \ . \tag{32}$$

The leading term in this nonlocal and energy dependent potential U_{eff} is $g_s\sigma + g_v V_o$, the sum of an attractive and a repulsive meson field. The third term in Eq. (31) is repulsive and lowers the overall attraction of the first two terms by almost 50% [7].

The Darwin potential and the energy-dependent terms in expression (31) do not contribute much if $\tilde{f}_A$ describes a single nucleon bound state. Neglecting the contribution from the small components, the scalar and the vector densities are identical. Considering now only the first three terms in U_{eff} the Eq. (30) corresponds to a Hartree problem where the nucleon-nucleon interaction is a density dependent one of Yukawa type.

$$V_{12}(z-z') = \frac{g_v^2}{2m_v} e^{-m_v|z-z'|}\left[1 - \frac{g_v^2}{2m\, m_v^2}\rho_v(z)\right] - \frac{g_s^2}{2m_s} e^{-m_s|z-z'|}\left[1 - \frac{g_s^2}{2m\, m_s^2}\rho_v(z)\right]. \tag{33}$$

To derive Eq. (33) we approximated one factor in the quadratic expressions in the third term of Eq. (31) due to the short range of the Greensfunctions in Eqs. (29) by

$$g_s\sigma = \frac{-g_s^2}{m_s^2}\rho_s \simeq \frac{-g_s^2}{m_s^2}\rho_v \tag{34a}$$

and

$$g_v V_o = \frac{g_v^2}{m_v^2}\rho_v \quad , \tag{34b}$$

respectively.

V. Initial Condition for Two Colliding Nuclear Slabs

As the Dirac equation (7) is Lorentz covariant the wave functions belonging to slabs which move with velocities -v and +v can be constructed from the above described static wave functions by the use of an inhomogeneous Lorentz transformation[15]. Characterizing the c.m. system of the colliding slabs by primes, one gets for the spinors at the time t' = 0 for the right slab

$$f'_\alpha(z',o) = e^{\frac{\omega}{2}\alpha_z} f_\alpha[\gamma(z'-z'_o), \frac{v}{c}\gamma(z'-z'_o)] \tag{35}$$

where

$$\gamma = \left(1 - \frac{v^2}{c^2}\right)^{-1/2}, \quad \tanh\omega = -\frac{v}{c} \tag{36}$$

α_z is the z-component of the $\vec{\alpha}$-matrix. z'_o is the central location of the right slab at t' = 0. z'_o has to be chosen large enough so that the slabs still do not interact with each other. Eq. (35) gives for the large and small components of the right slab up to a constant redundant phase factor at t' = 0

$$\tilde{f}'_{A_{jo}}(z',0) = \left\{\cosh\left(\frac{\omega}{2}\right)\tilde{f}_{A_{jo}}(\gamma(z'-z'_o)) + \sinh\left(\frac{\omega}{2}\right)\tilde{f}_{B_{jo}}(\gamma(z'-z'_o))\right\} e^{-i\varepsilon_{jo}\frac{v}{c}\gamma z'} \tag{37a}$$

$$\tilde{f}'_{B_{jo}}(z',0) = \left\{\sinh\left(\frac{\omega}{2}\right)\tilde{f}_{A_{jo}}(\gamma(z'-z'_o)) + \cosh\left(\frac{\omega}{2}\right)\tilde{f}_{B_{jo}}(\gamma(z'-z'_o))\right\} e^{-i\varepsilon_{jo}\frac{v}{c}\gamma z'} \tag{37b}$$

Here $\tilde{f}_{A_{jo}}$ and $\tilde{f}_{B_{jo}}$ are solutions of the static Dirac Eq. (19). As the collision problem is assumed to be symmetric with respect to the origin of the c.m. system, we can construct the spinors of the left slab using the parity operator P.

$$Pf'_\alpha(z',t') = i\gamma_0 f'_\alpha(z',t') \quad . \tag{38}$$

One can easily prove using Eqs. (37) and (13) that one gets for the right side slab the relations

$$\rho'_S(z',0) = \rho_S(z,0) \tag{39a}$$

$$\rho'_V(z',0) = \gamma\rho_V(z,0) \tag{39b}$$

$$j'_z(z',0) = -\frac{v}{c}\rho'_V(z',0) \tag{39c}$$

as one would expect. The kinetic energy per nucleon of two equal approaching slabs in the c.m. frame neglecting binding effects is

$$\frac{E_{cm}}{A} = m(\gamma - 1) \tag{40}$$

VI. Results and Discussion

Before we discuss the results we get in the TDRMF-model for the nuclear slab collision dynamics at different energies, we ask the question how reasonable the Lagrangian (1) with the above chosen parameter might be to describe nuclear collisions up to relativistically high energies.

At low energies of $E_{cm}/A < 5$ MeV, where during the collision the density increases to only slightly more than saturation density ρ_o, the Lagrangian (1) and the chosen parameters are certainly reasonable due to the fact that the structure of static nuclei is described fairly well. Even at moderately high energies $E_{cm}/A < 40$ MeV, one is encouraged by the excellent prediction for the energy dependence of the single particle mean potential.

For a nucleon of energy ε moving through symmetric infinite nuclear matter ($K_F = 1.34$ fm^{-1}) we obtain by solving the field Eqs. (5b) and (5c) for the mean potential of Eq. (31)

$$U_{eff} = -47.16 \text{ MeV} + 0.367(\varepsilon - m) - 5.325\ 10^{-4}(\varepsilon - m)^2/\text{MeV} \quad . \qquad (41)$$

Figure 4 shows the good agreement with the experimentally determined phenomenological real part of the optical potential[16] up to energies of 140 MeV. A comparison at even higher energies is difficult because of the not-well-known dispersion relation for U_{eff} [17].

At very high energies where $E_{c.m.}/A > 500$ MeV, the density during the slab collision might increase to more than $2\gamma\rho_o$ and the question arises how important three-, four-, etc. body interactions become. Such forces can be incorporated by a nonlinear scalar field[5,12] and a nonlinear vector field interaction. The nonlinear vector meson field might lead to a very strong repulsion for the penetrating slabs. At high bombarding

energies heavier mesons and nucleon resonances become certainly important and in principal could be included in the Lagrangian (1). Moreover, the existence of a pion field could contribute to the dynamics and, because of the time-dependent source terms, radiation of pions would occur.

Since the simple Lagrangian (1) might be not very reliable at very high bombarding energies, we restricted the energy domain we consider in this paper to $E_{c.m.}/A \leqslant 100$ MeV, which corresponds to a lab bombarding energy per nucleon of 421 MeV.

We discuss now the essential features of the results we get for the colliding slabs. To compare the low-energy results of the TDRMF-model with those of the TDHF-model we calculated the nuclear slab collision at the low energy of $E_{c.m.}/A = 3.5$ MeV and at the intermediate energies of $E_{c.m.}/A = 25$ MeV and 50 MeV. The results we get for the 3.5 MeV slab collision are shown in Fig. 5. This reaction typifies a deep inelastic process in which the system separates directly after having formed a compound system. The initial dynamics is characterized by only a slight increase in density due to the fact that the system has enough time to relax. Shortly before scission, density oscillations appear and, after the fragments have been formed, the density fluctuations slash back and forth in the two outcoming fragments. By calculating the half side momentum, we find that after separation the excitation per nucleon is about 2.4 MeV, which means that the process is strongly damped. An almost identical behavior for the density profiles of the slabs and a similar damping was found for the corresponding TDHF-calculation in ref. 14). For slab collisions at the intermediate energies of $E_{cm}/A = 25$ MeV and 50 MeV we find a different result (see Figs. 6 and 7). As in the TDHF-calculation the

central nuclear density increases to ~$1.7\rho_0$, however, the density profiles for the outcoming fragments look different. The characteristic of the TDHF-slab result at these energies is that after the compound system has formed, lumps appear at the nuclear surface and at least two of them separate off from the rest of the system. The velocity of the first lump is larger than the velocity of the incoming slab. In our case there is no lump formation at the surface. Instead of this, during the separation process of the slabs, a neck of matter between them is formed, which contracts to two clusters which move much slower than the primary fragments. At 100 MeV not even this is the case up to a time of $1.4\ 10^{-22}$ sec as shown in Fig. 8.

Up to now all the calculations have been done by neglecting the second time derivative in the Klein-Gordon Eqs. (14) assuming that retardation effects at these energies are still not very important. To see the influence of retardation, we have calculated the collision process for $E_{c.m.}/A = 100$ MeV by solving numerically the time dependent Klein-Gordon Eqs. (14) simultaneously with Eqs. (12). The result is shown as dashed lines in Fig. 8. The retardation effects smooth the density profile but do not lead to a different type of dynamics. The study of retardation effects at even higher energies is under investigation and we will report about these results elsewhere.

The slab dynamic is determined by the strength of the meson fields and the fermion spinors that are self-consistently coupled to them. Therefore, it is worthwhile to discuss the differences in the behavior of the meson fields at low and high slab bombarding energies. Figure 9 shows the scalar meson field as well as the space and time component of the vector meson field at three different moments during the collision process at

$E_{c.m.}/A$ = 3.5 MeV. The times considered here are at the beginning before the slabs touch, when they form a compound system and when they are almost separated again. Because of the symmetry of the problem, only one-half of the fields is drawn. In Fig. 10 these meson fields are plotted in the case of $E_{c.m.}/A$ = 100 MeV. As we know from the static slab calculation, the σ-field is in its absolute strength comparable to the V_0-field. The fact that the σ-field in its absolute value is slightly larger than the V_0-field leads to a bound nuclear slab system. Just so in the nuclear slab dynamics where the system is very sensitive to slight relative changes of the strengths of the meson fields. In Fig. 9 the sum of the scalar and vector field is always negative, which corresponds in a nonrelativistic Hartree-theory to an attractive single particle potential. In the case of $E_{C.M.}/A$ = 100 MeV, during the stage of penetration, the repulsive time component of the vector meson field becomes even larger than the absolute value of the scalar field. This leads to a net repulsion between both slabs. At even higher energies, these effects will become more dominant and an interesting dynamic of repelling slabs can be expected. Such a strong repulsion, which builds up rapidly in time when the slabs start to penetrate, leads to internal excitations of the system.

We find that the kinetic energy loss for the $E_{C.M.}/A$ = 100 MeV collision is about 12% and the slabs are therefore quite transparent. From heavy ion experiments at these energies, one would expect for a central collision a much more violent reaction. There are several reasons that might be responsible for this transparent behavior. One is that, due to the relativistic mean field approximation, the time dependent relativistic many-body state is at each time restricted to a single spinor Slater-determinant. This certaintly restricts the degrees of freedom of

the system and prohibits possible excitation modes. Another reason is the substantial omission of changes in the transverse direction due to the special slab geometry. In a realistic three-dimensional calculation where the transverse direction is not frozen, the mutual repulsion at high energies will lead to transverse instabilities and energy will flow into omitted modes. At $E_{c.m.}/A = 100$ MeV, the nucleon Δ-resonance will also contribute to the energy dissipation.

VII. Summary

We have shown that the TDRMF-model is very attractive to describe the dynamics of nuclear collisions since it describes the many-body collision problem from the basis of the relativistic quantum field theory. In this model the behavior of the fermion field is rather sensitive to small changes in the absolute size of the two meson fields. In the case of colliding nuclear slabs, the TDRMF-model agrees at low energies with corresponding calculations done in the TDHF-model.[14] For intermediate bombarding energies the TDRMF-model predicts a different dynamical behavior in the late stage of the reaction. Since this model is based on a relativistic quantum field theoretical concept, it includes at these intermediate energies already important relativistic effects. At the energy of $E_{c.m.}/A = 100$ MeV, there appears a net repulsion between the slabs but nevertheless the slabs are unrealistically transparent. This might be due to the omission of excitation modes in the mean field approximation, the restricted degrees of freedom in the special slab collision geometry, and to the incompleteness of the Lagrangian (1). We found that retardation effects do not modify the dynamical process considerably at an energy of 100 MeV.

Since we have shown that the slab collision problem in the TDRMF-model is numerically manageable, there are several very promising possibilities of future work.

First of all, to investigate the nuclear slab dynamics for even higher energies than reported here, using a more realistic Lagrangian, is of great interest. Furthermore, by including Δ-resonances, the effects of the recently theoretically proposed "Δ-resonance isomer"[18] on the collision dynamics could be studied. The question on the existence of a pion

condensate during a heavy ion collision and, particularly, its effects on the collision dynamics could be answered by including the pion field in the Lagrangian (1) as it was done in ref. 5) for static infinite nuclear matter. Moreover, as the fields change rapidly during the collision, they will act as a source for pion radiation. Beside this, the extension of the calculations to a realistic three-dimensional computation is certainly desirable.

Acknowledgments

The author has benefited from very helpful discussions and technical support throughout the course of his work from S. Bohrmann. He wishes to thank J. Boguta for conversations during the early stage of the project. He is especially grateful for the discussions he could have with N.K. Glendenning and his encouraging support and to the HISS group who made the computational work possible by placing their VAX-computer to his proposal. He would like to express his thanks to the Nuclear Science Theory group at the Lawrence Berkeley Laboratory for the kind hospitality extended to him. He further acknowledges the support of the Deutsche Forschungsgemeinschaft, W.-Germany, Bonn-Bad Godesberg. This work was also supported by the Director, Office of Energy Research, Division of Nuclear Physics of the Office of High Energy and Nuclear Physics of the U.S. Department of Energy under Contract W-7405-ENG-48.

Appendix

Numerical methods for solving self-consistently the static slab problem

For $A/F = 1.4\ fm^{-2}$ and $K_\perp = 0$ the system of Eqs. (19) by using Eqs. (28) and (29) with the constraint (26) is solved self-consistently. By denoting with $k\,\Delta z$ the space coordinate at the mesh point k and using for the space derivatives a two point formula, the Eqs. (19) become

$$-\frac{1}{\Delta z}\left(\hat{f}_{B_k} - \hat{f}_{B_{k-1}}\right) + F_k \tilde{f}_{A_k} = \epsilon \tilde{f}_{A_k} \tag{A1a}$$

$$\frac{1}{\Delta z}\left(\tilde{f}_{A_{k+1}} - \tilde{f}_{A_k}\right) + G_k \hat{f}_{B_k} = \epsilon \hat{f}_{B_k} \tag{A1b}$$

where

$$F_k = g_v V_{o_k} + |m_k^*| \quad , \quad G_k = g_v V_{o_k} - |m_k^*| \ . \tag{A2}$$

The use of the right side two point difference formula in (A1a) and the left side difference formula in (A1b) has the advantage to write Eqs. (A1) easily in form of an eigenvalue problem where the matrix is a symmetric band matrix with only two off diagonals. The boundary conditions for the functions $\tilde{f}_A$ and $\hat{f}_B$ are included by the fact that the matrix we diagonalize is of finite dimension.[19] For the mesh size we choose $\Delta z = 0.25$ fm; the z-coordinate interval is [-12 fm, 12 fm].

To calculate the integrals in Eqs. (29) we use the same method the authors of ref. 14)* used to determine their Hartree-potential. With this at each mesh point k the second order finite difference approximation is used for the scalar and vector densities. The scalar and vector fields

---

*There in formula A7 for $X_{q=0}$ the factor 2 has to be deleted.

can then be expressed as a sum over integrals times the corresponding density at different mesh points. The integrals themselves can easily be calculated analytically. As the equation for the scalar field is an integral equation, we find the solution by iterations. Calculating first ρ_s^i by using a previous σ^{i-1}, we determine with Eq. (29a) a new σ^i and repeat this procedure five times, which is in our case sufficient. We found that the iterative solution for the densities is very much improved by using the average of the two most recent solutions

$$\bar{\rho}_{s/v}^{i+1} = \frac{1}{2}\left(\rho_{s/v}^{i} + \rho_{s/v}^{i+1}\right) . \tag{A3}$$

We start the iteration using for the vector density the result for the nuclear density in the corresponding Hartree-calculation of ref. 14). The scalar density is assumed to be 0.93 times the vector density. After 36 iterations we find a precision for the densities at each mesh point of $\sim 10^{-4}$. For the energies the accuracy is about the same.

Numerical methods for solving the time dependent equations

We solve the system (12), which is coupled by the meson fields to the Klein-Gordon Eqs. (14) for $K_\perp = 0$, by using an implicit difference method.[20] For the time and space derivatives at the space-time point $(k\Delta z, n\Delta t)$ we take the mid point formula. The functions $\tilde{f}_A$ and $\tilde{f}_B$ in the Eqs. (12) are replaced by their mean values determined by the earlier and later time step. With this one obtains

$$\frac{1}{c\Delta t}\left(\bar{f}_{A_k}^{n+1} - \bar{f}_{A_k}^{n-1}\right) + \frac{1}{\Delta z}\left(\bar{f}_{B_{k+1}}^{n} - \bar{f}_{B_{k-1}}^{n}\right) - ig_v V_{z_k}^{n}\left(\bar{f}_{B_k}^{n+1} + \bar{f}_{B_k}^{n-1}\right)$$

$$= -i\left(g_v V_{o_k}^{n} + \left|m_k^{*n}\right| - m\right)\left(\bar{f}_{A_k}^{n+1} + \bar{f}_{A_k}^{n-1}\right) \tag{A4a}$$

$$\frac{1}{c\Delta t}\left(\overline{f}^{n+1}_{B_k} - \overline{f}^{n-1}_{B_k}\right) + \frac{1}{\Delta z}\left(\overline{f}^{n}_{A_{k+1}} - \overline{f}^{n}_{A_{k-1}}\right) - ig_v V^n_{z_k}\left(\overline{f}^{n+1}_{A_k} + \overline{f}^{n-1}_{A_k}\right)$$

$$= -i\left(g_v V^n_{o_k} - \left|m^{*n}_k\right| - m\right)\left(\overline{f}^{n+1}_{B_k} + \overline{f}^{n-1}_{B_k}\right) . \qquad \text{(A4b)}$$

Here

$$\tilde{\overline{f}} = e^{-imct}\,\overline{f} \quad . \qquad \text{(A5)}$$

With this replacement, one gets rid of the fast time oscillations of the relativistic wave function caused by the rest-mass of the nucleons.

We resolve the system (A4) with respect to the real and imaginary parts of $\overline{f}^{n+1}_{A_k}$ and $\overline{f}^{n+1}_{B_k}$. To stabilize the above algorithm we replace after having determined $\overline{f}^{n+1}$ the functions $\overline{f}^{n}$ by

$$\overline{f}^{n} \leftarrow \frac{1}{4}\left(\overline{f}^{n+1} + 2\overline{f}^{n} + \overline{f}^{n-1}\right) \qquad \text{(A6)}$$

and recalculate $\overline{f}^{n+1}$.

As the system is symmetric with respect to the origin of the c.m. frame, we have to calculate only those spinors that belong initially to the right side slab. The remaining spinors are determined by using the parity operator of Eq. (38).

At low and intermediate bombarding energies, retardation effects are believed to be less important. In these cases we solve simultaneously with Eqs. (A4) the Klein-Gordon equations (14) by neglecting the second time derivative in the D'Alembert-operator. This means we use Eqs. (29) and the corresponding one for the space component V_z of the vector meson field.

For the high slab collision energy $E_{c.m.}/A = 100$ MeV, we take the correct D'Alembert-operator in the Klein-Gordon Eqs. (14) into account to see what the effect of retardation is. The time-dependent Klein-Gordon

equations are solved numerically by using the difference scheme proposed by Courant et al.[21]. Instead of solving the Klein-Gordon equation

$$\frac{1}{c^2}\frac{\partial^2 U}{\partial t^2} - \frac{\partial^2 U}{\partial z^2} + M^2 U = \rho \tag{A7}$$

(U is now representative for the meson fields, M for their masses, and ρ for the scalar- and vector density or the current) one can calculate the equivalent coupled system of partial differential equations, namely

$$\frac{1}{c}\frac{\partial U}{\partial t} + \frac{\partial U}{\partial z} = V \tag{A8a}$$

$$\frac{1}{c}\frac{\partial V}{\partial t} - \frac{\partial V}{\partial z} = -M^2 U + \rho \quad . \tag{A8b}$$

Using forward time differences, central space differences, and substituting U_k^n, V_k^n, and ρ_k^n by their average values[22], which one gets from the adjacent left and right space mesh points, the scheme that results from Eqs. (A8) is

$$U_k^{n+1} = [(1 - r)U_{k+1}^n + (1 + r)U_{k-1}^n + (V_{k+1}^n + V_{k-1}^n)c\Delta t]/2 \tag{A9a}$$

$$V_k^{n+1} = [(1+r)V_{k+1}^n + (1-r)V_{k-1}^n - M^2(U_{k+1}^n + U_{k-1}^n)c\Delta t + (\rho_{k+1}^n + \rho_{k-1}^n)c\Delta t]/2 \tag{A9b}$$

here $r = c\Delta t/\Delta z$.

The initial conditions for U and V are determined by the approaching slabs which move with constant velocity.

A criterion for the accuracy of the algorithm described above is the change of the metric of the relativistic wave functions and the change of the total energy of the system during the slab collision. The mesh sizes (Δz, $c\Delta t$) we have chosen, which give as we think sufficient accuracy and computation time still does not become prohibitive, are in units of fm for E_{cm}/A = 3.5 MeV: ($0.25/\gamma$, $1.25\ 10^{-2}$), for 25 MeV: ($0.25/\gamma$, $1.25\ 10^{-2}$),

for 50 MeV: $(0.125/\gamma,\ 6.25\ 10^{-3})$, and for 100 MeV: $(0.125/\gamma,\ 4.4\ 10^{-3})$. Here γ is the γ-factor of Eq. (36). Therefore, a typical calculation involves between 200 400 points in z and 8000 to 16000 steps in time. Until the end of the reaction where the slabs are well separated again, the metric of the spinors changed less than 1%. The total energy of the system changed by less than ±0.4%.

The neglect of the second derivative in the Klein-Gordon Eqs. (14) in those cases in which we do not consider retardation effects causes that the expression (17) for the total energy is no longer a strictly conserved quantity. Adding formally the amount of energy change, one gets an expression in terms of the fields that is strictly conserved. For the numerical computation of the energy and momentum in Eqs. (17) and (18), the time derivatives are approximated by two point backward differences and for the space derivatives mid point differences are used. The integration was done by using Simpson's 1/3-rule. To determine the initial wave functions when we use the mesh size $\Delta z = 0.125$ fm a quadratic two side interpolation is used.

References

1. A.K. Kerman, Proceedings of the International School of Physics "Enrico Fermi", Course LXIX (1976) 135
2. Y. Yariv, Z. Fraenkel, Phys. Rev. C,20, 2227 (1979)
3. H. Stöcker, J. Hofmann, J.A. Maruhn and W. Greiner, Progress in Particle and Nuclear Physics (Pergamon Press), Vol. 4, pp. 133-195 (1980)
4. J.D. Walecka, Ann. Phys. 83 (1974) 491
5. B. Banerjee, N.K. Glendenning and M. Gyulassy, Nucl. Phys. A361 (1981) 326
6. F.E. Serr and J.D. Walecka, Phys. Lett. 79B (1978) 10
7. J. Boguta, LBL-11894 preprint (December 1980), submitted to Nucl. Phys. A and LBL-11466 preprint (August 1980), submitted to Phys. Lett. B
8. M. Jaminon, C. Mahaux and P. Rochus, Phys. Rev. C,22 (1980) 2027
9. M.H. Johnson and E. Teller, Phys. Rev. 98 (1955) 783
10. H.P. Duerr, Phys. Rev. 103 (1956) 469
11. S.A. Chin, Ann. Phys. 108 (1977) 301
12. J. Boguta and A.R. Bodmer, Nucl. Phys. A292 (1977) 413
13. G. Wentzel, Quantum Theory of Fields, Interscience Publishers, New York, 1949
14. P. Bonche, S. Koonin and J.W. Negele, Phys. Rev. C,13 (1976) 1226
15. J.D. Bjorken and S.D. Drell, Relativistic Quantum Mechanics (1964), McGraw Hill, New York
16. M.M. Giannini, G. Ricco and A. Zucchiatti, Lecture Notes in Physics 89 (1979) 126
17. G. Passatore, Nucl. Phys. A110 (1980) 91

18. J. Boguta, LBL-preprint, to be published

19. F. Scheid, Schaum's outline of theory and problems of numerical analysis, McGraw-Hill, New York (1968)

20. E. Isaacson and H.B. Keller, Analysis of Numerical Methods, Wiley, 1966

21. R. Courant, E. Isaacson and M. Rees, Comm. Pure Appl. Math. 5 (1952) 243

22. R.D. Richtmyer, Differences Methods for Initial Value Problems (Interscience), New York, 1957

Table 1

j	1	2	3	4
$\epsilon_{jo} - m$ (MeV)	-74.15	-59.60	-41.54	-23.56
$K_{\perp max}(j)$ (fm^{-1})	1.336	1.173	0.933	0.606

Single particle energies ϵ_{jo} and the maximum occupied transverse momenta $K_{\perp max}(j)$.

Figure captions

Fig. 1. The large component $\tilde{f}_{A_{jo}}$ (full curve) and the small component $\hat{f}_{B_{jo}}$ (dashed curve) of the four different relativistic nuclear wave functions with $K_\perp = 0$ for the static slab. The small component is stretched by the factor 10.

Fig. 2. Nucleon density $\rho_v(z)$ and scalar density $\rho_s(z)$ for the static slab of $A/F = 1.4$ fm^{-2}.

Fig. 3. The scalar field $g_s\sigma(z)$ and the time component of the vector field $g_v V_o(z)$ for the static slab of $A/F = 1.4$ fm^{-2}.

Fig. 4. The experimentally found energy-dependent depth of the real part of the optical potential and the single nucleon potential U_{eff} of Eq. (31).

Fig. 5. Nucleon density profiles $\rho_v(z,t)$ for two colliding nuclear slabs for $E_{c.m.}/A = 3.5$ MeV at different times in units of 10^{-21} s. The total A/F is 2.8 fm^{-2}. Retardation effects are not taken into account.

Fig. 6. The same as in Fig. 5 for $E_{c.m.}/A = 25$ MeV.

Fig. 7. The same as in Fig. 5 for $E_{c.m.}/A = 50$ MeV.

Fig. 8. The nucleon density profiles $\rho_v(z,t)$ for two colliding nuclear slabs for $E_{c.m.}/A = 100$ MeV at different times in units of 10^{-21}s. The total A/F is 2.8 fm^{-2}. The full curves show the results without taking retardation effects into account. The dashed curves show the results if the Klein-Gordon equations for the meson fields are solved exactly.

Fig. 9. The scalar field $g_s\sigma(z,t)$ and the space and time components of the vector fields $g_v V_z(z,t)$ and $g_v V_o(z,t)$ at three different times during the reaction for $E_{c.m.}/A = 3.5$ MeV. The time is in units of 10^{-21}s.

Fig. 10. The same as in Fig. 9 at a bombarding energy of $E_{c.m.}/A = 100$ MeV.

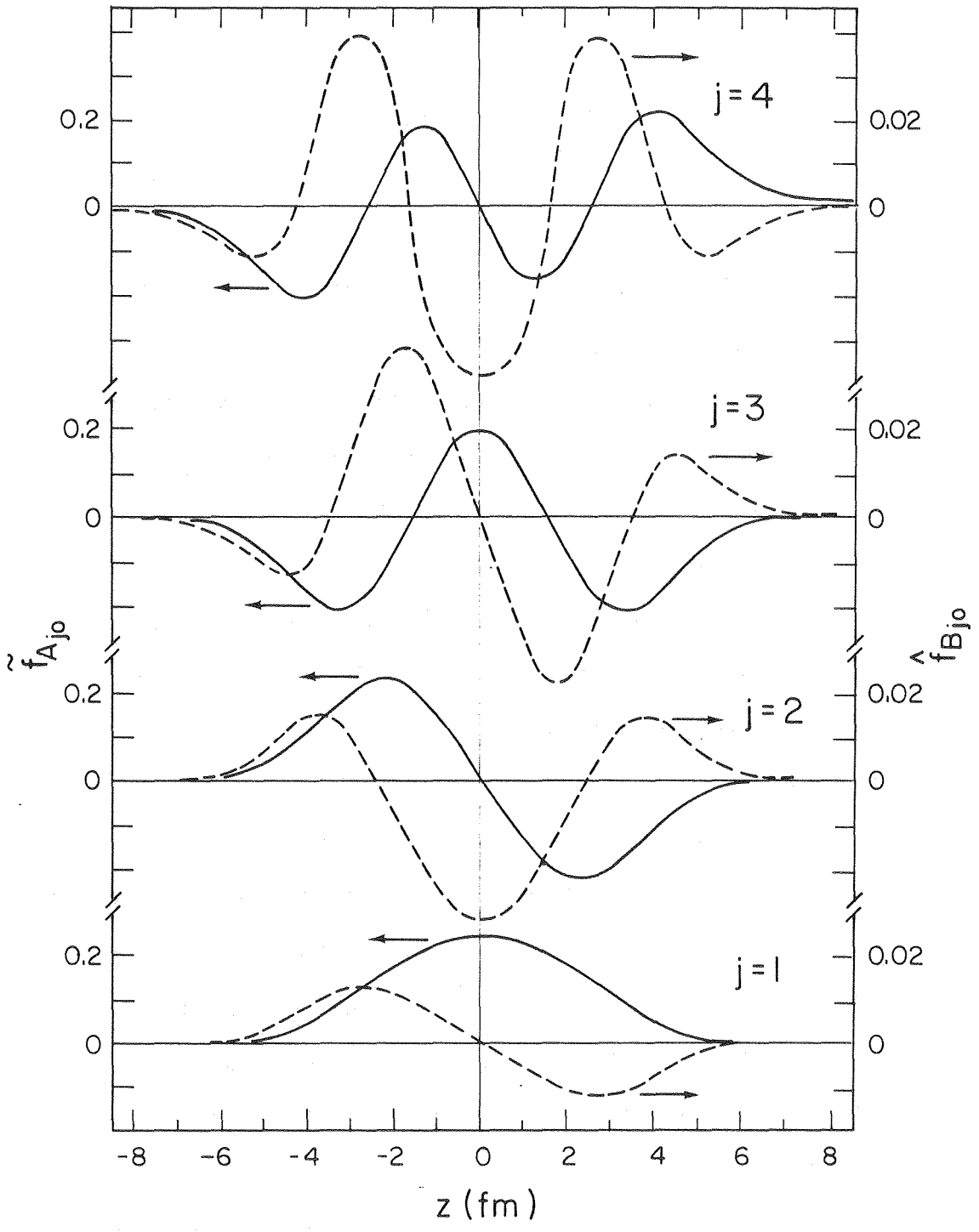

XBL 814 - 4575

Fig. 1

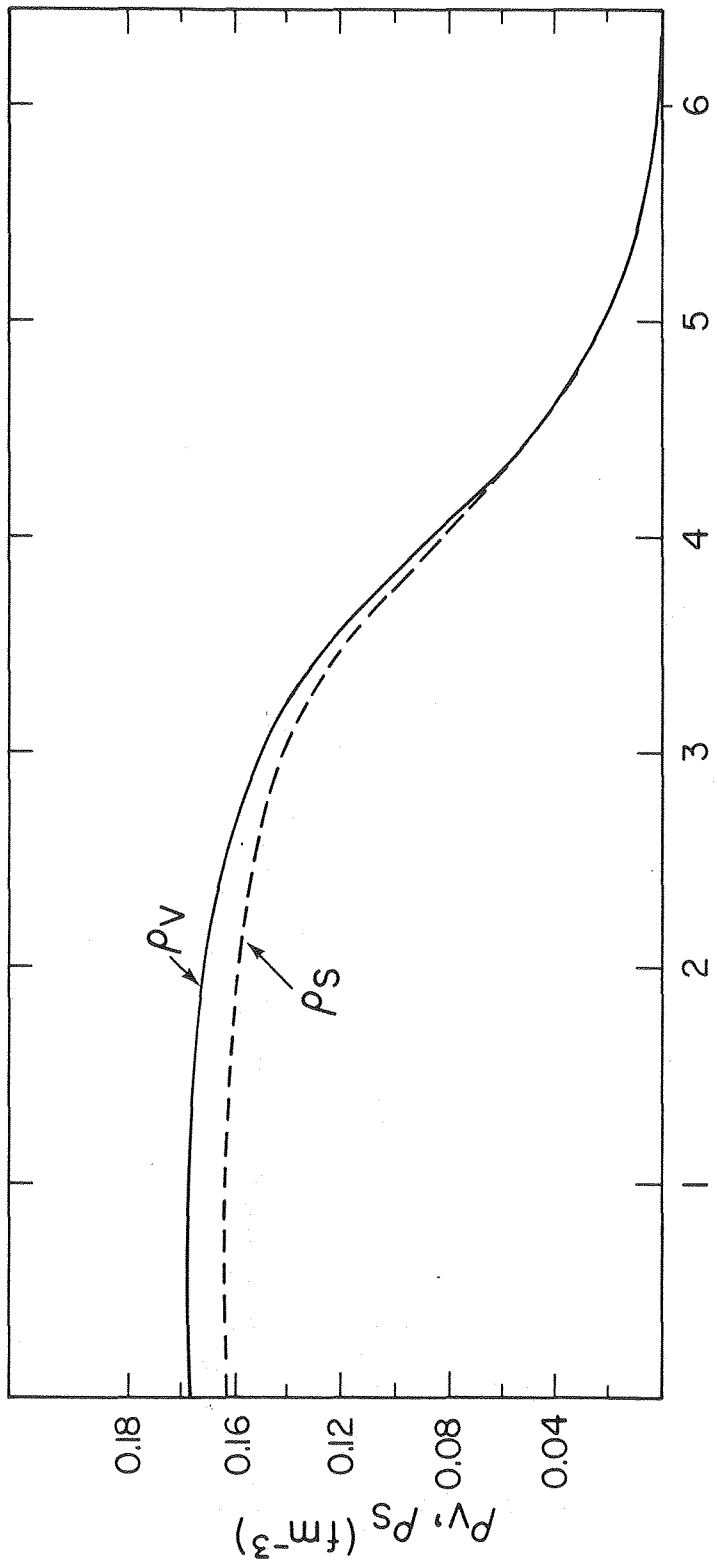

XBL 814-4573

Fig. 2

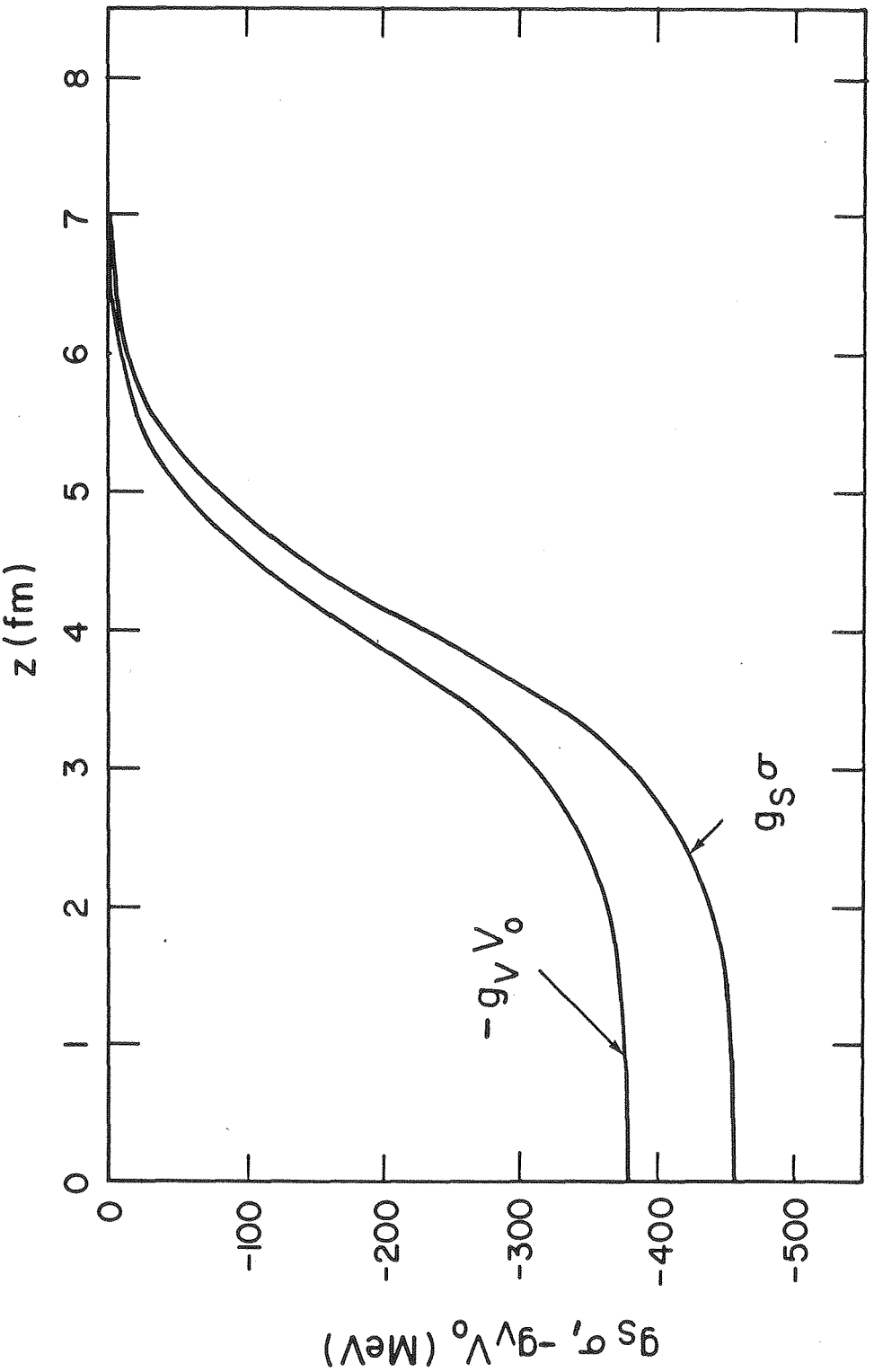

XBL 814-4572

Fig. 3

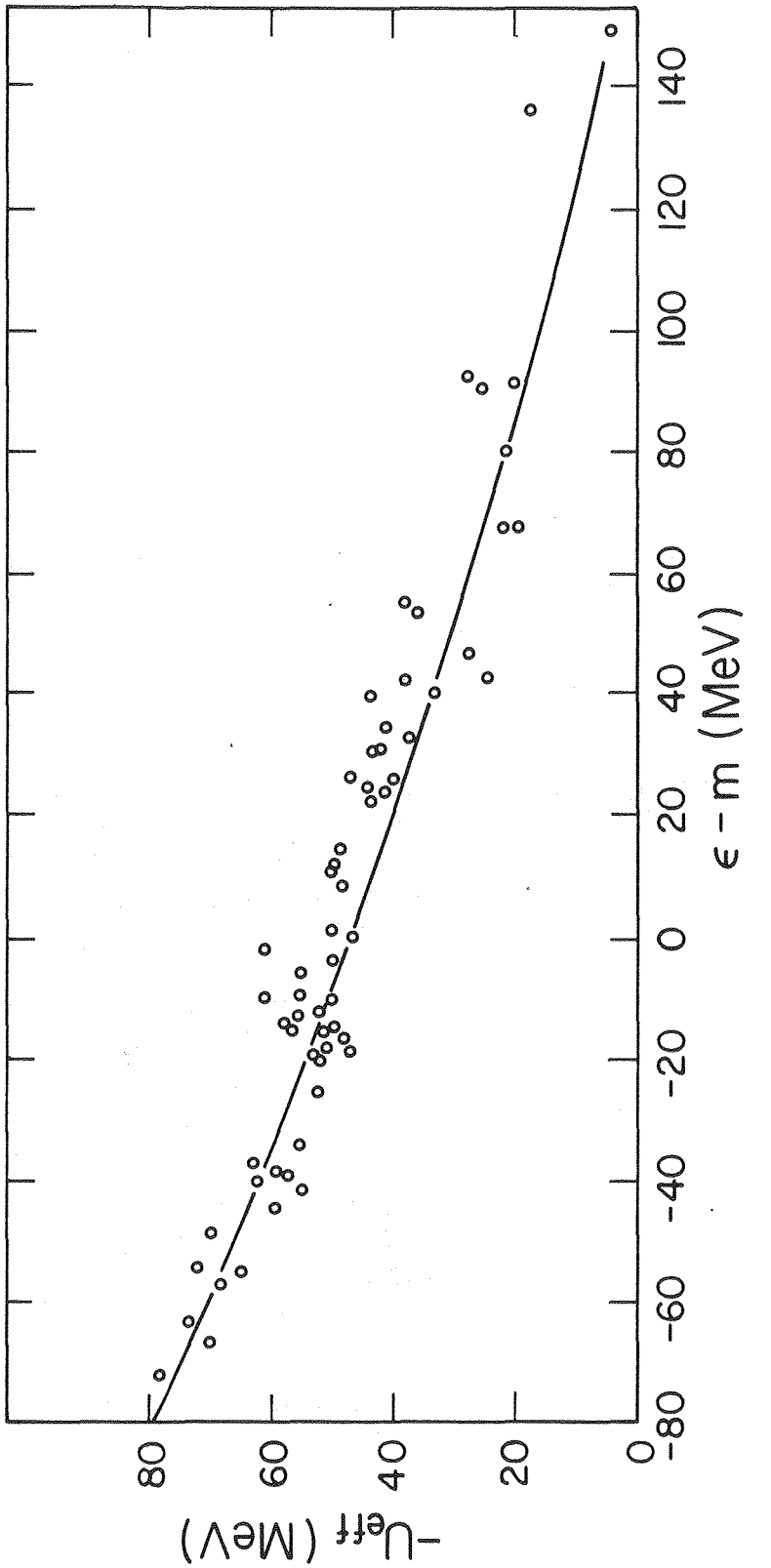

XBL 814-4571

Fig. 4

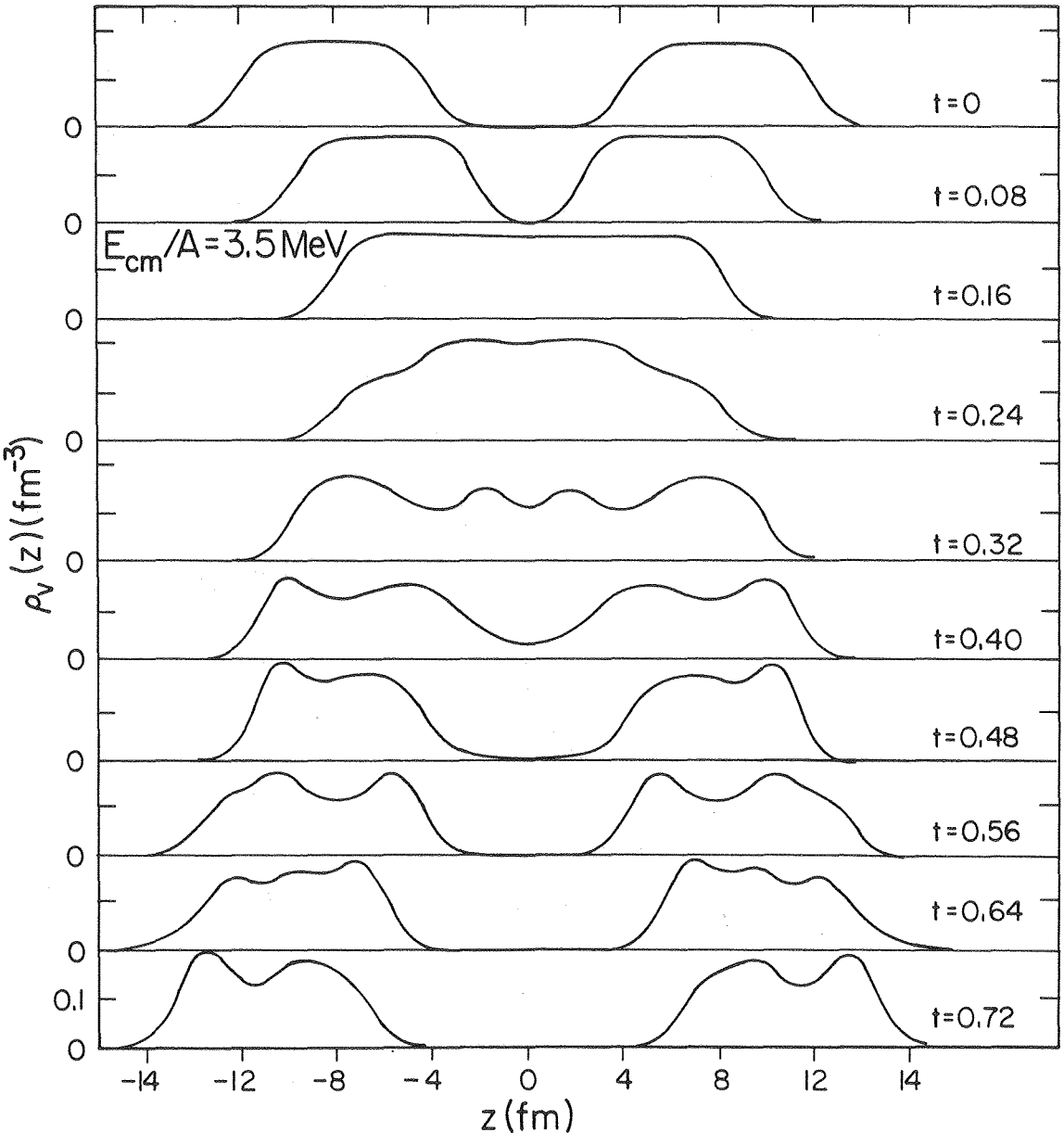

XBL 814-4569

Fig. 5

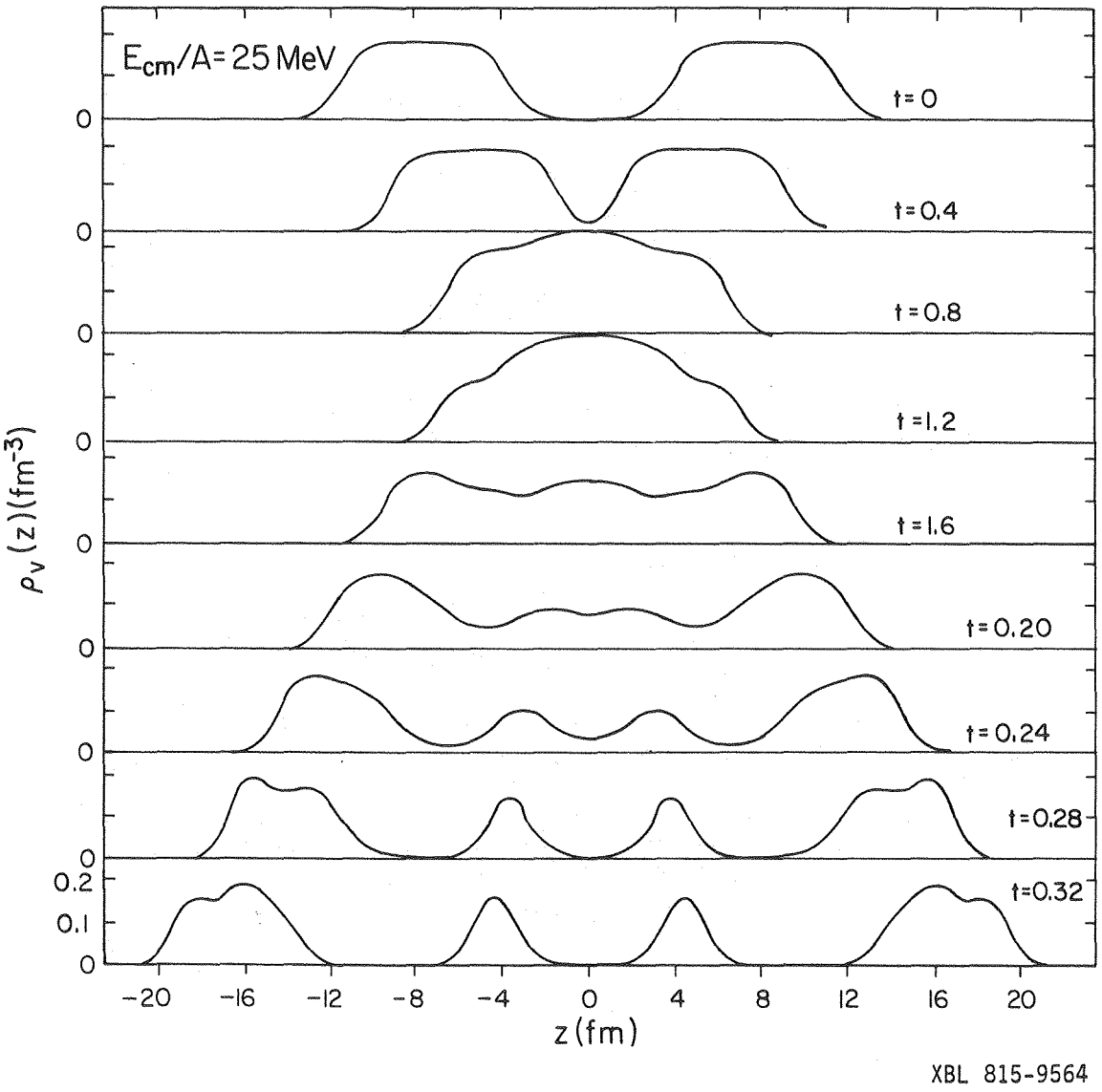
$E_{cm}/A = 25$ MeV
t = 0
t = 0.4
t = 0.8
t = 1.2
t = 1.6
t = 0.20
t = 0.24
t = 0.28
t = 0.32
$\rho_v(z)(fm^{-3})$
0
0.2
0.1
−20
−16
−12
−8
−4
0
4
8
12
16
20
z (fm)
XBL 815-9564

Fig. 6

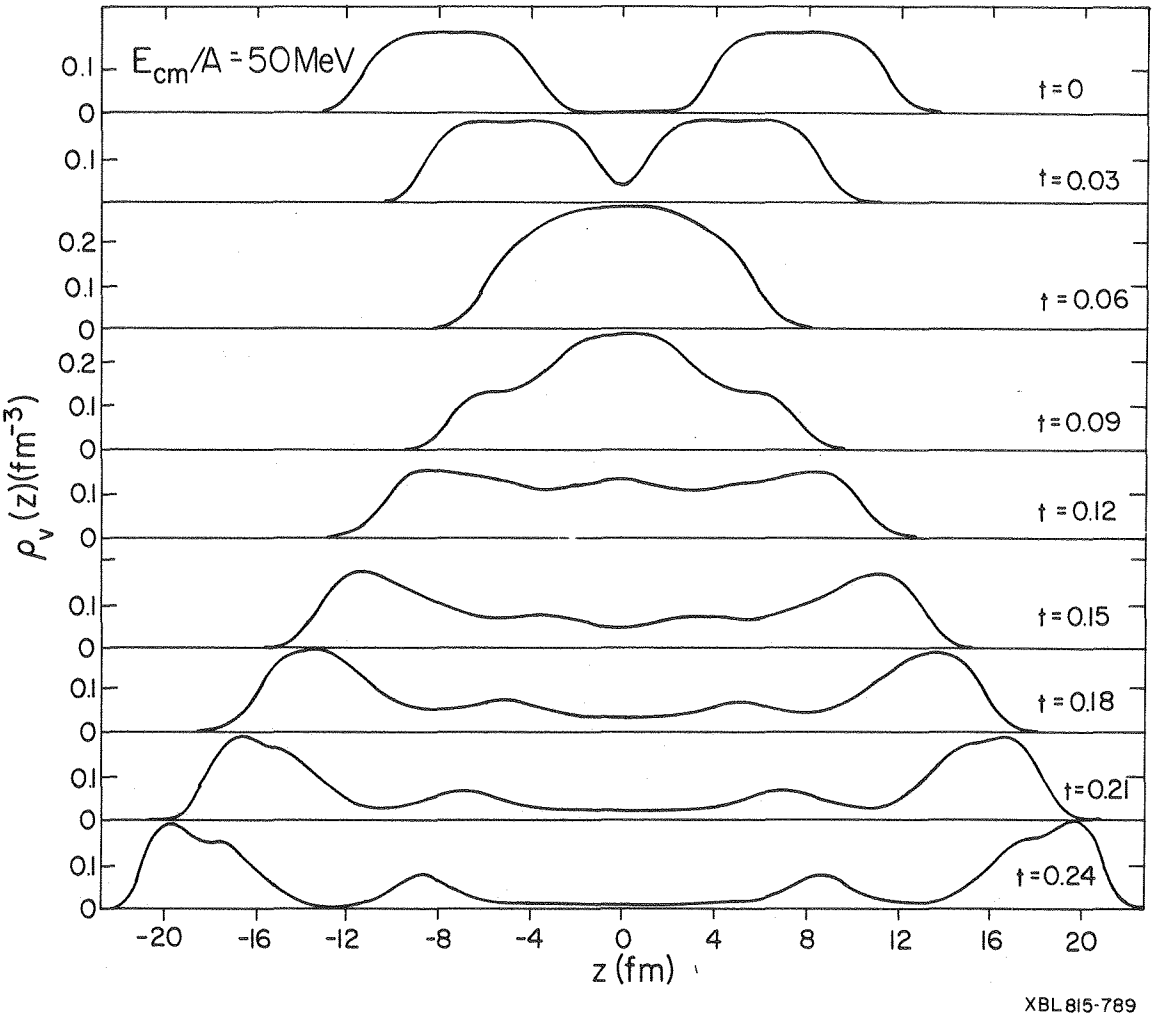
$E_{cm}/A = 50$MeV
t = 0
t = 0.03
t = 0.06
t = 0.09
t = 0.12
t = 0.15
t = 0.18
t = 0.21
t = 0.24
$\rho_v(z)(fm^{-3})$
z (fm)
XBL 815-789

Fig. 7

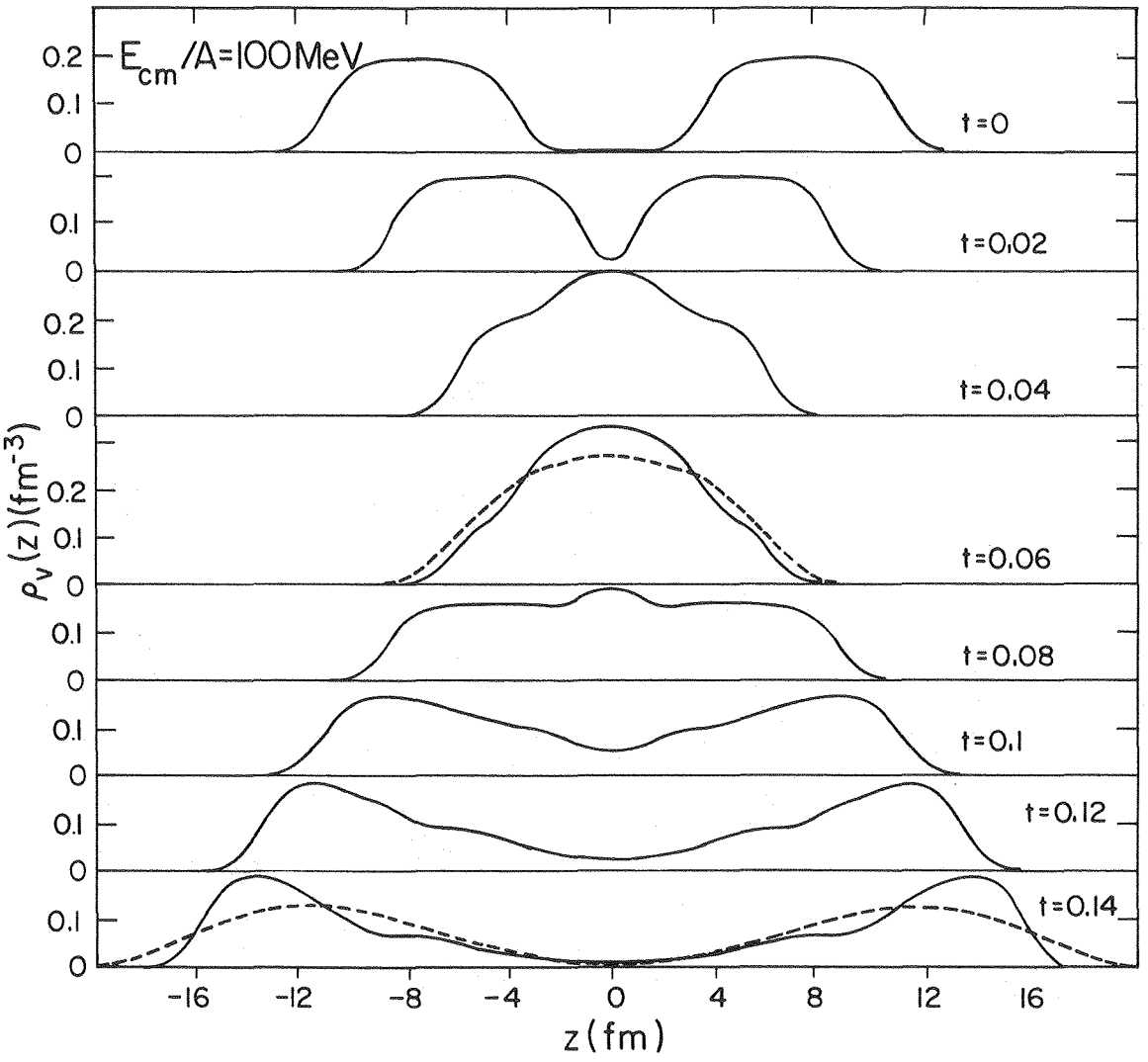

XBL 814-4570A

Fig. 8

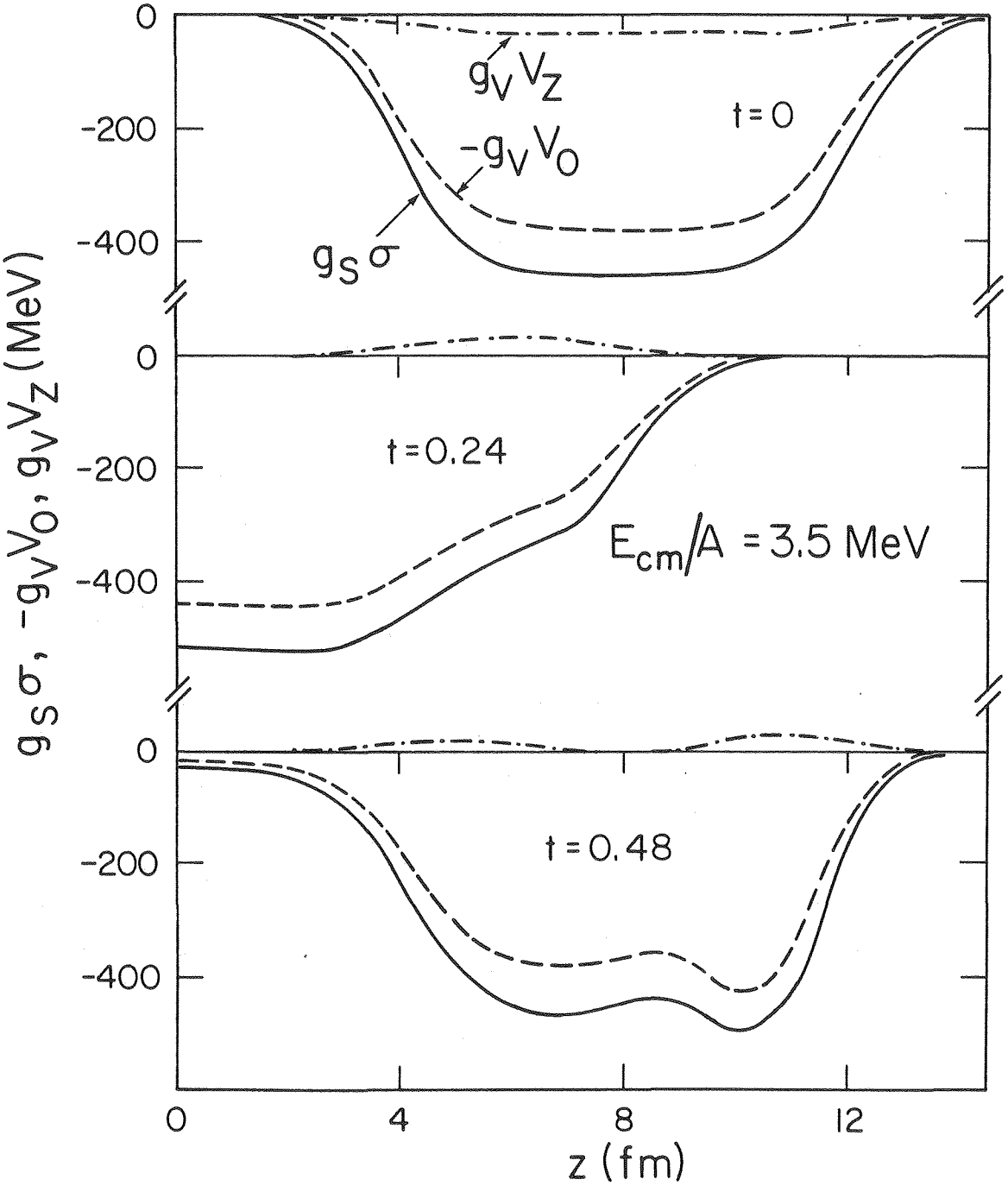

XBL 815-9563

Fig. 9

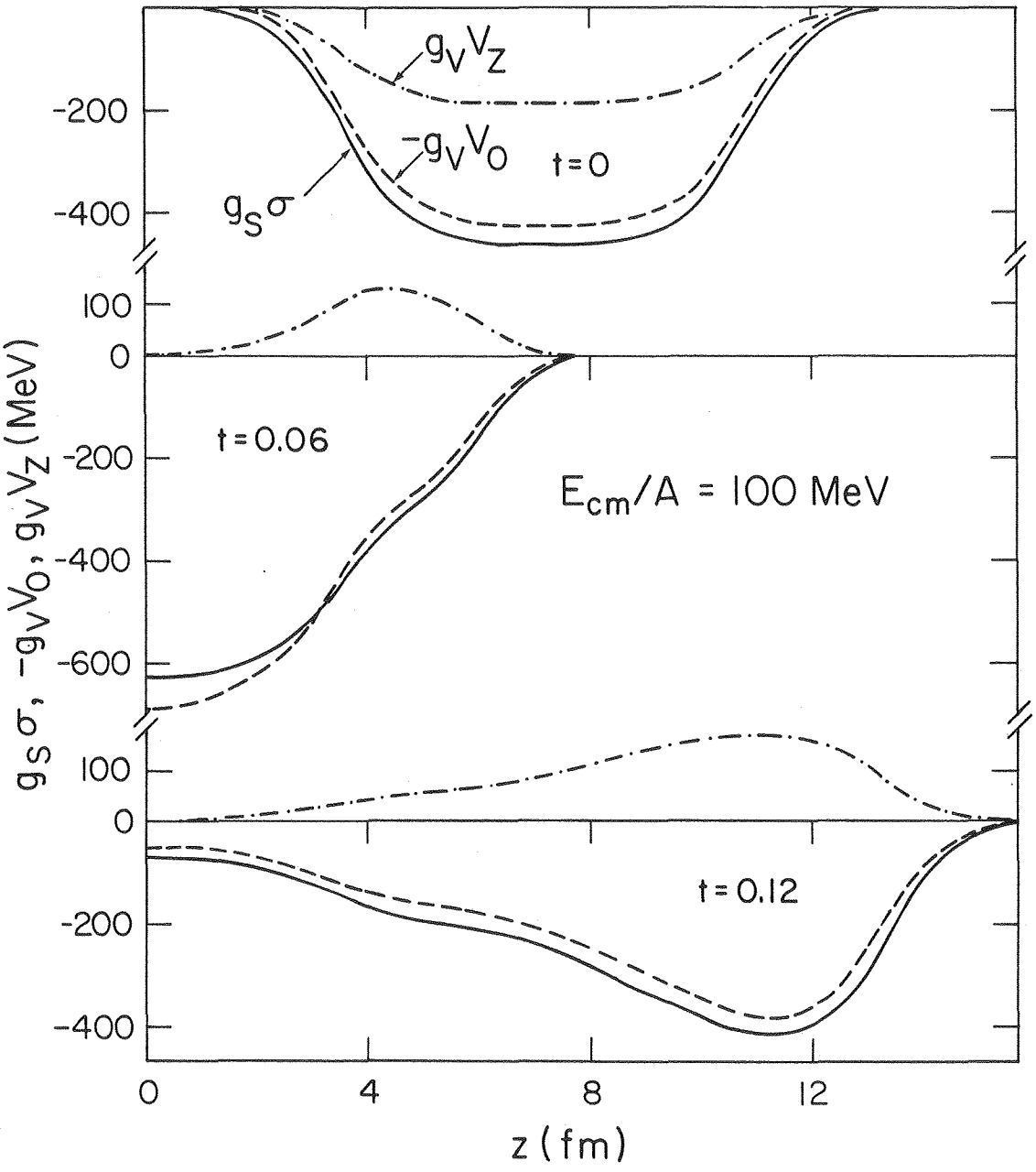

XBL 814-4576

Fig. 10